Event-Triggered T-S Fuzzy Load Frequency Control With Variable Probabilistic Release for Renewable Energy Integrated Power Systems

Zhou Gu, *Senior Member, IEEE*, Yujian Fan, Fan Yang, and Engang Tian, *Senior Member, IEEE*

***Abstract*— This paper explores a T-S fuzzy-model-based approach for load frequency control in network-based power systems under random false data injection attacks, taking into account the integration of electric vehicles and photovoltaic power generation systems. Amidst uncertainties in parameters and nonlinear items of integrated power systems, a T-S fuzzy model is formulated, enabling convenient design and analysis of the rolling horizon optimal control (RHOC) strategy with variable control gains to ensure mean-square asymptotic stability in power systems. Considering the broad dispersion of new energy generation systems across the power grid, the use of network communication has become crucial. To overcome the limitation of network bandwidth while ensuring frequency stability, a novel event-triggered mechanism employing a varying probabilistic release strategy (VPRS) within grouped triggered data-packets is proposed for transmitting power frequency signals. Initially, a conventional event-triggered mechanism is established to generate primary triggering packets, stored in a buffer until designated packet capacity of the group is reached. Then, following the probabilistic updating algorithm in RHOC strategy, the transmission task is executed upon the arrival of the final triggered packet within each group. The efficacy of the proposed method is validated through a numerical example.**

***Note to Practitioners*—This paper introduces a T-S fuzzy-model-based RHOC strategy for power systems with renewable energy, addressing challenges posed by limited communication resources and random false data injection attacks. The innovative event-triggered mechanism with a VPRS optimizes network utilization for power systems, while the RHOC strategy with variable control gains guarantees mean-square asymptotic stability despite uncertainties and nonlinearities within the power network. While the efficacy of the approach is demonstrated through numerical examples, practitioners should take into account practical constraints, such as scalability issues and the complexities involved in real-world implementation. Future research will focus on enhancing scalability and addressing implementation challenges to facilitate broader adoption in power systems.**

***Index Terms*— VPRS-based event-triggered mechanism, T-S fuzzy integrated power systems, load frequency control.**

Received 8 September 2024; accepted 10 October 2024. Date of publication 29 October 2024; date of current version 26 March 2025. This article was recommended for publication by Associate Editor R. Carli and Editor Q. Zhao upon evaluation of the reviewers' comments. This work was supported in part by the National Natural Science Foundation of China under Grant 62273183 and Grant 62103193, in part by the Startup Funding of Anhui Polytechnic University under Grant 2024YQQ001, and in part by the Natural Science Foundation of Jiangsu Province of China under Grant BK20231288. *(Corresponding author: Zhou Gu.)*

Zhou Gu is with the School of Electrical Engineering, Anhui Polytechnic University, Wuhu 241000, China (e-mail: gzh1808@163.com).

Yujian Fan and Fan Yang are with the College of Mechanical & Electronic Engineering, Nanjing Forestry University, Nanjing 210037, China (e-mail: fanyujian0505@163.com; yfan0510@sina.cn).

Engang Tian is with the School of Optical-Electrical and Computer Engineering, University of Shanghai for Science and Technology, Shanghai 200093, China (e-mail: tianengang@163.com).

Digital Object Identifier 10.1109/TASE.2024.3486093

I. Introduction

In THE swiftly advancing landscape of the electrical era, a myriad of novel energy products have surfaced, prompting an escalating significance in the investigation of power systems. This emphasis is particularly pronounced in the domain of large power systems, where the integration of diverse new energy components, such as electric vehicles (EVs), photovoltaic power generation systems (PPGSs), and wind power, have garnered substantial attention, emerging as the focal point within contemporary research endeavors. The load frequency control (LFC) problem in a power system that integrates thermal power and PPGSs was investigated in [1]. In [2], single-area and multi-area power systems that integrate wind power and EVs were constructed to study the frequency deviation caused by intermittent wind power generation. The investigation in [3], [4] explored the LFC issue faced by hybrid power systems incorporating EVs and being vulnerable to denial-of-service (DoS) attacks. PPGSs and EVs represent crucial elements in endeavors aimed at energy conservation and emission reduction. Consequently, there is practical significance in exploring the stability of power systems incorporating these components. Such considerations inspire the research on this power system with PPGSs and EVs in this paper.

Frequency serves as the crucial performance metric in evaluating power systems [5], [6]. The stability of the power system will be compromised when the load frequency fluctuation of the system exceeds the acceptable range. LFC plays a pivotal role in preserving the frequency within a stable domain. Consequently, investigating LFC is an essential endeavor for the comprehensive study of any power system. Recent advancements have significantly contributed to addressing the LFC problem [7], [8], [9], [10]. For example, Cooperative LFC strategies were investigated for multi-area power systems using a multi-agent deep reinforcement learning method in [7] and an observer-based method in [8].

In [9], [10], AI methods were used to mitigate the impact of false data injection (FDI) attacks on the LFC system.

The fluctuating and uncertain nature of EVs and PPGS, introducing nonlinear characteristics or unknown models, presents a considerable challenge in designing an effective LFC strategy. To tackle this challenge, the T-S fuzzy model emerges as a potent mathematical tool capable of approximating nonlinear systems using a series of fuzzy rules and membership functions. Through the incorporation of linguistic variables and the principles of fuzzy logic, the T-S fuzzy model adeptly represents and comprehends the inherent dynamic behaviors within power systems. This facilitates the development of efficient decision-making and control strategies. For example, in [4], a switching interval type-2 fuzzy power model was established to address the LFC problem in nonlinear multi-area power systems. Wang et al. proposed a T-S fuzzy model to ensure frequency security in an interconnected power system incorporating wind farms in [11]. This paper will leverage these modeling methodologies to design a networked LFC strategy for power systems.

Network communication has emerged as an indispensable element within power systems due to the widespread deployment of new energy generation systems across the grid. Past studies, as exemplified by [12], [13], have emphasized the cost-effectiveness and flexibility inherent in modern network-based mechanisms. Consequently, a well-designed communication scheme has become imperative for network-based power systems. Despite the previous prevalence of the time-triggered mechanism [14] in the field of LFC, a significant volume of redundant data packets wast the network resource. To tackle this challenge, researchers proposed event-triggered mechanisms (ETMs) [15], [16], [17], [18], [19], [20]. Under these mechanisms, only data packets that meet the specified triggering conditions are permitted for release into the network. Up to now, the ETMs are categorized broadly into static ETMs [21], [22], dynamic ETMs [23], [24], and other atypical triggering mechanisms [25], [26]. For example, a static ETM-based wide-area power system model containing DoS and deception attacks was constructed and controlled using a predictive damping controller in [22]. A dynamic ETM with dynamic parameters and an error-related exponential term was designed in [23] to further reduce data release rates for the power system. An integral-based ETM that integrates history information was proposed in [25] to reduce redundant signals. Notably, when historical information is weighted and averaged into the triggering condition, the resulting ETM is termed a memory-based ETM, as evidenced in studies such as [26], [27], [28].

Within existing ETMs, triggering conditions are often formulated as relative event triggering conditions, comparing the error between the packets at the current sampling instant and those at the last triggered instant [20], [21]. However, under the existing ETM, even when the system tends toward stability, a considerable number of redundant data packets are released into the network. Concerning the LFC issue, when the power system tends to stabilize, the output signal undergoes minimal changes, rendering the random selection of one packet from multiple triggered packets, while discarding the rest irrelevant packets. Conversely, during the power system fluctuations, this random selection could significantly affect the stability of the power system. To address this challenge, a reasonable feedback mechanism is crucial for the LFC in power systems, thereby mitigating the impact of discarding a substantial number of triggered signals. Hence, the primary motivation of this paper is to explore a probabilistic ETM that fulfills such a critical requirement.

In addition, cyber-attacks are a critical problem that cannot be ignored in power control systems [16], [29], [30], [31], [32]. Substantial research efforts have been dedicated to this area, yielding significant outcomes. For instance, LFC strategies considering FDI attacks, system disturbances, and time delays were formulated for the power system in [9], [30]. FDI and DoS attacks are considered in the network-based multi-area power system, and the H_∞ LFC scheme were developed to stabilize the frequency of the power system in [31]. In [33], a detection and defense strategy was proposed against FDI attacks. Despite these efforts, the LFC problem within power systems subjected to FDI attacks remains an insufficiently explored domain.

Based on the aforementioned discussions, this paper addresses the trade-off problem between control performance and communication limitations in power systems integrating EVs and PPGSs. An innovative VPRS-based ETM is proposed to save network resources, under which an RHOC strategy with an probabilistic updating algorithm is designed to achieve improved performance. The main contributions in this paper are summarized as follows:

1) A T-S fuzzy model is established to address the perturbations and nonlinear characteristics arising from the integration of EVs and PPGSs into real-world power systems. Unlike most existing studies, such as [1], [2], which typically rely on deterministic linear models for renewable energy sources, our approach provides a more flexible and robust control design that adapts to the uncertainties and nonlinearities exhibited by EVs and PPGSs in real-world power grid scenarios.
2) An innovative VPRS-based ETM is introduced for LFC systems, aimed at further reducing network throughput while maintaining LFC performance. In comparison to the traditional ETM, such as the one in [20], this communication mechanism further selects the triggered data packets and ensures the efficient transmission of crucial information by the proposed RHOC strategy.
3) An RHOC strategy is developed to enhance the control performance of LFC power systems. Under this strategy, the release probability of the triggered packet is determined by the proposed probabilistic updating algorithm. Before the start of the next packet group, the fuzzy controller gains are updated, resulting in the system that adapts more effectively compared to traditional fuzzy controllers with fixed gains, as observed in [34], [35].

The remainder of this paper is organized as follows: The system and communication modeling are presented in Section II. The main results of the co-design of the LFC and the VPRS-based ETM are given in Section III. A practical example using the proposed VPRS-based ETM is provided in

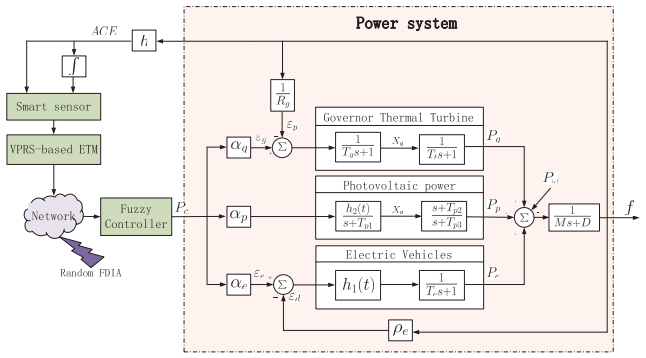

Fig. 1. Framework of VPRS ETM-based power system with PPGSs and EVs.

TABLE I
SYMBOLS AND MEANINGS IN FIG. 1

Symbols	Meanings
f, P_p	Deviations of frequency and output power in PPGSs.
ACE, P_c	Area control error, control input.
D	Load damping coefficient.
P_ω	External disturbances.
X_g, P_g, P_e	The incremental changes in governor valve position, turbine output powers, and EVs.
T_{p1}, T_{p3}	Opposite values of the abscissa for the pole point.
b, M	Frequency bias constant, inertia constant.
$h_2(t)$, $h_1(t)$	Variable gains of PPGSs and EVs.
T_{p2}	Opposite values of the abscissa for the zero point.
X_p	Transition power deviation.
T_g, T_t, T_e	Time constants of speed governor, turbine, and EVs.
ρ_e, R_g	Droop characteristic of EVs and governor.
α_g, α_p, α_e	Participation factors of turbine, PPGSs, and EVs.

Section IV to demonstrate the validity of theoretical results. The main works are concluded in Section V.

Notation: In this paper, some symbols are defined as follows: $A^TBA = \mathfrak{T}\{A, B\}$; $\mathbf{He}\{X\} = X^T + X$; $\mathfrak{N}_l = \{1, 2, \ldots, l\}$; $\mathfrak{C}_{s=1}^{l}\{Q_s\}(\mathfrak{C}_l\{Q\}) = [Q_1^T, Q_2^T, \ldots, Q_l^T]^T([\underbrace{Q^T, Q^T, \ldots, Q^T}_{l}]^T)$; $\mathfrak{C}\{A, B\} = [A^T, B^T]^T$; $\mathbf{diag}\{A, B\} = \begin{bmatrix} A & 0 \\ 0 & B \end{bmatrix}$; $\mathbf{diag}_l\{A\} = \mathbf{diag}\{\underbrace{A, A, \ldots, A}_{l}\}$; $\mathbf{diag}_{m=1}^{l}\{A_m\} = \mathbf{diag}\{A_1, A_2, \ldots, A_l\}$; $\mathfrak{S}\{A_{11}, *; A_{21}, A_{22}\} = \begin{bmatrix} A_{11} & * \\ A_{21} & A_{22} \end{bmatrix}$, where $*$ is denoted by A_{21}^T.

II. System and Communication Modeling

A. T-S Fuzzy Model of Power Systems

LFC is essential for maintaining the grid's stability by ensuring the power generated matches the power consumed. Any imbalance may result in power outages or damage to equipment. In this study, an LFC power system that includes traditional thermal power system, PPGSs, and EVs is considered, as depicted in Fig. 1. The feedback control signal, frequency, is transmitted over the network which is subject to random FDI attacks.

Borrowing models of traditional thermal power systems in [29], PPGSs in [1] and EVs in [14], we present the following related dynamic equations of the power system:

$$\begin{cases} \dot{f}(t) = -\dfrac{D}{M}f(t) + \dfrac{1}{M}\big(P_g(t) + P_p(t) + P_e(t) - P_\omega(t)\big), \\ \dot{X}_g(t) = -\dfrac{1}{T_g R_g}f(t) - \dfrac{1}{T_g}X_g + \dfrac{\alpha_g}{T_g}P_c(t), \\ \dot{P}_g(t) = \dfrac{1}{T_t}X_g(t) - \dfrac{1}{T_t}P_g(t), \\ \dot{X}_p(t) = -T_{p1}X_p(t) + \alpha_p h_2(t)P_c(t), \\ \dot{P}_p(t) = (T_{p2} - T_{p1})X_p(t) - T_{p3}P_p(t) + \alpha_p h_2(t)P_c(t), \\ \dot{P}_e(t) = -\dfrac{\rho_e h_1(t)}{T_e}f(t) - \dfrac{1}{T_e}P_e(t) + \dfrac{\alpha_e h_1(t)}{T_e}P_c(t), \\ \dot{\mathscr{E}}(t) = bf(t) \end{cases} \tag{1}$$

where the meanings of symbols are given in Table I.

Let's define $x(t) = [f(t)\ X_g(t)\ P_g(t)\ X_p(t)\ P_p(t)\ \ P_e(t)\ \mathscr{E}(t)]^T \in \mathbb{R}^7$, $y(t) = [f(t)\ \mathscr{E}(t)]^T \in \mathbb{R}^2$, $u(t) = P_c(t)$ and $\omega(t) = P_\omega(t) \in \mathbb{R}$, where $x(t)$, $y(t)$, $u(t)$ and $\omega(t)$ denote the state, output, control input and external disturbance of the power systems, respectively. From these definitions, we derive the following state equation for the power system with integrated new energy generation systems:

$$\begin{cases} \dot{x}(t) &= Ax(t) + B_u u(t) + B_\omega \omega(t), \\ y(t) &= Cx(t) \end{cases} \tag{2}$$

where

$$A = \begin{bmatrix} -\frac{D}{M} & 0 & \frac{1}{M} & 0 & \frac{1}{M} & \frac{1}{M} & 0 \\ -\frac{1}{T_g R_g} & -\frac{1}{T_g} & 0 & 0 & 0 & 0 & 0 \\ 0 & \frac{1}{T_t} & -\frac{1}{T_t} & 0 & 0 & 0 & 0 \\ 0 & 0 & 0 & -T_{p1} & 0 & 0 & 0 \\ 0 & 0 & 0 & T_{p2} - T_{p1} & -T_{p3} & 0 & 0 \\ -\frac{\rho_e h_1(t)}{T_e} & 0 & 0 & 0 & 0 & -\frac{1}{T_e} & 0 \\ b & 0 & 0 & 0 & 0 & 0 & 0 \end{bmatrix},$$

$$B_u = \begin{bmatrix} 0 & \frac{\alpha_g}{T_g} & 0 & \alpha_p h_2(t) & \alpha_p h_2(t) & \frac{\alpha_e h_1(t)}{T_e} & 0 \end{bmatrix}^T,$$

$$B_\omega = \begin{bmatrix} -\frac{1}{M} & 0 & 0 & 0 & 0 & 0 & 0 \end{bmatrix}^T,$$

$$C = \begin{bmatrix} 1 & 0 & 0 & 0 & 0 & 0 & 0 \\ 0 & 0 & 0 & 0 & 0 & 0 & 1 \end{bmatrix}.$$

Notice that the output power of PPGSs is subject to fluctuations due to varying light intensity at different time instances. Consequently, the gain $h_2(t)$ of PPGSs in (2) exhibits temporal variation characterized by a trigonometric function-like form. Similarly, the quantity of EVs fluctuates over time, leading to a non-monotonic time-varying gain $h_1(t)$. These variations typically demonstrate nonlinear features within a certain range. In this study, we assume $h_1(t) \in [\check{H}_1\ \ \hat{H}_1]$ and $h_2(t) \in [\check{H}_2\ \ \hat{H}_2]$.

To address the aforementioned challenge, the T-S fuzzy model method proves to be instrumental. Drawing inspiration from the approach outlined in [36], the representations of $h_1(t)$ and $h_2(t)$ take the following form:

$$\begin{cases} h_1(t) = S_1(h_1(t))\hat{H}_1 + S_2(h_1(t))\check{H}_1 \\ h_2(t) = Z_1(h_2(t))\hat{H}_2 + Z_2(h_2(t))\check{H}_2, \end{cases} \tag{3}$$

where $h_r(t)$, $r \in \{1, 2\}$ is the premise variable. Define the following membership functions (MFs):

$$S_1(h_1(t)) = \frac{h_1(t) - \check{H}_1}{\hat{H}_1 - \check{H}_1}, \quad S_2(h_1(t)) = \frac{\hat{H}_1 - h_1(t)}{\hat{H}_1 - \check{H}_1},$$
$$Z_1(h_2(t)) = \frac{h_2(t) - \check{H}_2}{\hat{H}_2 - \check{H}_2}, \quad Z_2(h_2(t)) = \frac{\hat{H}_2 - h_2(t)}{\hat{H}_2 - \check{H}_2}. \tag{4}$$

Obviously, the MFs satisfy:

$$S_1(h_1(t)) + S_2(h_1(t)) = 1, \quad Z_1(h_2(t)) + Z_2(h_2(t)) = 1.$$

Combining (2)-(4), the r-th rule of T-S fuzzy-based power system for the system in (1) can be represented by:
Plant Rule i: **IF** $h_1(t)$ is $S_r(h_1(t))$ and $h_2(t)$ is $Z_r(h_2(t))$, **THEN**

$$\begin{cases} \dot{x}(t) = A_i x(t) + B_{ui} u(t) + B_\omega \omega(t), \\ y(t) = Cx(t) \end{cases}$$

where $r \in \{1,\ 2\}$, $i \in \{1,\ 2,\ 3,\ 4\}$.

By utilizing center-average defuzzifier, the system (1) can be converted to the following T-S fuzzy model

$$\begin{cases} \dot{x}(t) = \sum_{i=1}^{4} \mu_i\big(h(t)\big)[A_i x(t) + B_{ui} u(t) + B_\omega \omega(t)], \\ y(t) = Cx(t) \end{cases} \tag{5}$$

where

$$\mu_1(h(t)) = S_1(h_1(t)) \times Z_1(h_2(t)),$$
$$\mu_2(h(t)) = S_1(h_1(t)) \times Z_2(h_2(t)),$$
$$\mu_3(h(t)) = S_2(h_1(t)) \times Z_1(h_2(t)),$$
$$\mu_4(h(t)) = S_2(h_1(t)) \times Z_2(h_2(t)),$$

and $\mu_i(h(t)) \geq 0$, $\sum_{i=1}^{4} \mu_i(h(t)) = 1$.

B. VPRS-Based ETM

Before designing the VPRS-based ETM, a conventional ETM is presented

$$t_{k+1}h = t_k h + \min_{v \in N_+} \{vh | \psi\big(y(t_k h), e_y(t), t\big) > 0\}, \tag{6}$$

where $\psi\big(y(t_k h), e_y(t), t\big) = \mathfrak{T}\{e_y(t), \Xi\} - \theta\mathfrak{T}\{y(t_k h), \Xi\}$, $e_y(t) = Ce(t)$, $e(t) = x(t_k h) - x(t_k h + vh)$, $\theta \in (0, 1)$ is a given constant, and $\Xi > 0$ is a weight matrix to be designed.

The ETM in (6) has been extensively utilized in numerous existing results. However, its application usually leads to the transmission of a significant amount of redundant data over the network, particularly when the system is approaching stability. To overcome this limitation, we propose a two-step VPRS-based ETM approach. During the first step, primary triggering packets (PTPs) are generated through the implementation of a traditional ETM. These PTPs are then directed to a buffer that can hold l data-packets. During the second step, a pre-designed probabilistic updating algorithm is employed to select the final release packets (FRPs) from these PTPs.

In this study, $r_n h$, d_n, and τ_n denote the actual triggered instant, the waiting delay, and the network-induced delay in the n-th group, respectively, and it is assumed that $\max\{\tau_n + d_n + h\} = \tau_M$. Then, the new divided triggered interval is $\mathcal{T}_n = [r_n h + d_n + \tau_n,\ r_{n+1}h + d_{n+1} + \tau_{n+1})$.

Here, we define $\delta_m^n(t)$ with $m \in \mathfrak{N}_l$ that denotes the transmission probability of the m-th triggered packet in the n-th group. For $\delta_m^n(t)$ with different m, it is assumed that they are independent and identically distributed random variation governed by $0-1$ distribution, and have the following properties:

$$\sum_{m=1}^{l} \delta_m^n(t) = 1; \mathbb{E}\{\delta_m^n(t)\} = \bar{\delta}_m^n; \mathbb{E}\{(\delta_m^n(t) - \bar{\delta}_m^n)^2\} = (\hat{\delta}_m^n)^2,$$

where l is a given positive integer.

For achieving better control performance, the RHOC strategy is developed for the transmission probability:

$$\bar{\delta}_m^{n+1} = \frac{\|y(t_{k+m}h) - y(r_n h)\|}{\sum_{m=1}^{l} \|y(t_{k+m}h) - y(r_n h)\|}, \tag{7}$$

where $t_{k+m}h$ with $m \in \mathfrak{N}_l$, $k = (n-1)(l-1)$ and $\bar{\delta}_m^{n+1}$ are the m-th packet in the $n+1$ group and its transmission probability, respectively.

For a clearer understanding of the proposed VPRS-based ETM, consider the time sequence example illustrated in Fig. 2 where $l = 3$. In this example, it is evident that $\{y(t_k h)\}_{k=1,2,3,\cdots}$ are selected as triggered packets. Every 3 consecutive PTPs (marked with green triangle), such as $\{y(t_1 h),\ y(t_2 h),\ y(t_3 h)\}$, $\{y(t_3 h),\ y(t_4 h),\ y(t_5 h)\}$, $\cdots$, are subsequently grouped sequentially into the buffer during the first step. In the second step, $\{y(r_n h)\}_{n=1,2,3,\cdots}$ is identified as the FRPs (marked with purple hexagon in Fig. 2) utilizing the proposed RHOC strategy outlined in (7).

Remark 1: It is noted that there is a common packet between the adjacent group (for example, $y(t_7 h)$ in Fig. 2 is both in the third group and in the fourth group). However, it cannot be the FRP both of these two groups, since the transmission probability of the first triggered packet in the fourth group $\bar{\delta}_1^4$ is $\|y(t_7 h) - y(r_3 h)\| / \sum_{m=1}^{l} \|y(t_{6+m}h) - y(r_3 h)\| = 0$.

Remark 2: The selection of the value l is determined by system stability requirements and the specific situation. Generally, as the l value increases, computational complexity rises, making it more challenging to satisfy stability conditions. Conversely, a smaller value l brings the communication mechanism closer to traditional ETMs. Specifically, the VPRS-based ETM will reduce to traditional ETMs if l in (8) is set to 1. In this example, $l = 3$ is selected as it represents a balanced case and can be extended to scenarios where $l > 3$ is required.

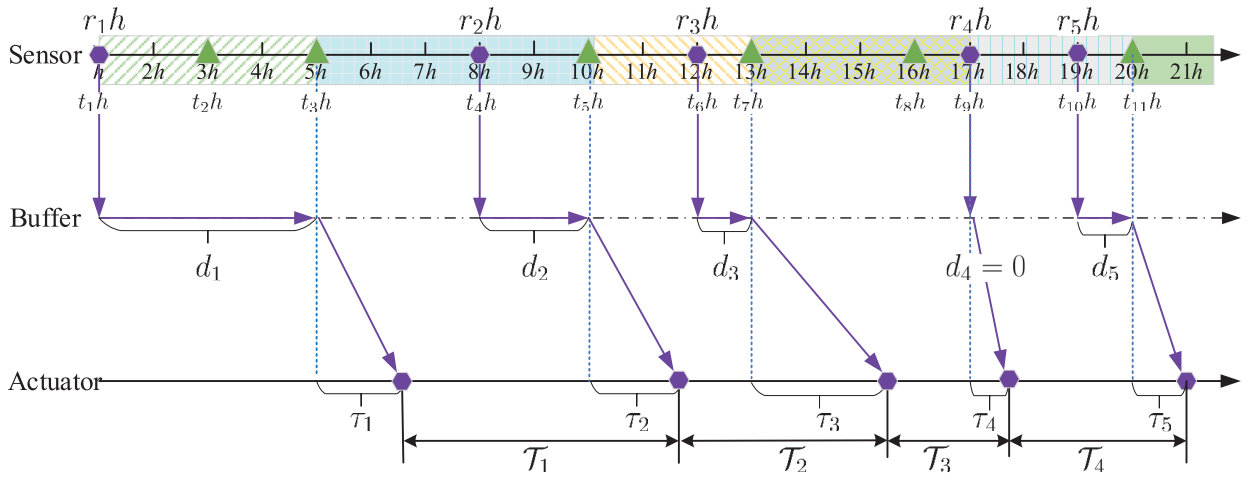

Fig. 2. Sequence schematic diagram of VPRS-based ETM with $l = 3$.

Based on the above discussion, the VPRS-based ETM is constructed as

$$t_{k+m+1}h = t_{k+m}h + \min_{v\in N_+}\{vh|\Psi\big(y(t_{k+m}h), e^n_{ym}(t), t\big) > 0\}, \tag{8}$$

where $m \in \mathfrak{N}_l$, and $\Psi\big(y(t_{k+m}h), e^n_{ym}(t), t\big) = \mathfrak{T}\{e^n_{ym}(t), \Xi\} - \theta\mathfrak{T}\{y(t_{k+m}h), \Xi\}$; $e^n_{ym}(t) = Ce^n_m(t)$, $e^n_m(t) = x(t_{k+m}h) - x(t_{k+m}h + vh)$ is the m-th error in the n-th group.

Similar to [20], we define

$$\tau^n_m(t) = t - t_{k+m}h - vh, \tag{9}$$

$$e^n_{ym}(t) = y(t_{k+m}h) - y(t - \tau^n_m(t)) = C(x(t_{k+m}h) - x(t - \tau^n_m(t))) \tag{10}$$

for $t \in \mathcal{T}_n$, $m \in \mathfrak{N}_l$. For convenience, $e^n_m(t) \triangleq x(t_{k+m}h) - x(t - \tau^n_m(t)$, then, one has $e^n_{ym}(t) = Ce^n_m(t)$.

Then, for $t \in \mathcal{T}_n$, we have

$$y(t) = y(r_nh) = C\sum_{m=1}^{l-1}\delta^n_m\Pi^n_m(t) + C(1 - \sum_{m=1}^{l-1}\delta^n_m)\Pi^n_l(t), \tag{11}$$

where $\Pi^n_m(t) = e^n_m(t) + x(t - \tau^n_m(t))$.

Now, we can design the following T-S fuzzy-based output feedback control (OFC) for the power system in (5):

Control rule j: **IF** $h_1(t)$ is $S_r(h_1(t))$ and $h_2(t)$ is $Z_r(h_2(t))$, **THEN**

$$u(t) = K_j y(r_nh)$$

for $t \in \mathcal{T}_n$, $n \in N$.

Similarly, the overall fuzzy OFC can be represented by

$$u(t) = \sum_{j=1}^{4}\mu_j\big(h(r_nh)\big)K_j y(r_nh), t \in \mathcal{T}_n, \tag{12}$$

where K_j, $j \in \mathfrak{N}_4$ are the controller gains to be designed.

Taking into account the asynchronous nature of the premise variables before and after network processing, following the insights from [37], we suppose that the MF satisfies

$$\mu_j\big(h(r_n)\big) > \kappa_j\mu_j\big(h(t)\big). \tag{13}$$

C. Model of Random FDI Attacks

Due to the new energy generation systems across wide areas, wireless communications have become susceptible to attacks from malicious adversaries. As shown in Fig. 1, after being attack the control input in (12) becomes

$$u(t) = \sum_{j=1}^{4}\mu_j\big(h(r_nh)\big)K_j[\chi(t)p(y(t)) + y(r_nh)] \tag{14}$$

for $t \in \mathcal{T}_n$, where $p(y(t))$ represents the FDI attack signal. It is assumed that the FDI attack signal satisfies that

$$\|p(y(t))\|_2 \le \|\mathcal{M}y(t)\|_2 \tag{15}$$

where $\mathcal{M}$ is a constant matrix. In (14), $\chi(t) \in \{0, 1\}$ is a random variable. When $\chi(t) = 1$, it signifies a successful attack by the adversary, whereas $\chi(t) = 0$ denotes a failed or ineffective attack at that time. In addition, $\chi(t)$ is assumed to satisfy

$$\mathbb{E}\{\chi(t)\} = \bar{\chi}, \mathbb{E}\{(\chi(t) - \bar{\chi})^2\} = \hat{\chi}^2.$$

Remark 3: Some approaches to modeling FDI attacks require detailed information about power systems, as seen in [9]. In contrast, the model in (15) does not require such information, making it widely used in the existing literature.

Considering the attack, the control input in (14) can be rewritten as

$$\begin{aligned} u(t) = &\sum_{j=1}^{4}\mu_j\big(h(r_nh)\Big\{\bar{\chi}K_jp(y(t)) + (\chi(t) - \bar{\chi})K_jp(y(t)) \\ &+ \sum_{m=1}^{l-1}\bar{\delta}^n_mK_jC\Pi^n_m(t) + \sum_{m=1}^{l-1}(\delta^n_m(t) - \bar{\delta}^n_m)K_jC\Pi^n_m(t) \\ &+ (1 - \sum_{m=1}^{l-1}\bar{\delta}^n_m)K_jC\Pi^n_l(t) + \sum_{m=1}^{l-1}(\bar{\delta}^n_m - \delta^n_m(t))K_jC\Pi^n_l(t)\Big\}. \end{aligned} \tag{16}$$

D. Closed-Loop System With VPRS-Based ETM

Combining (5), (11) and (16) yields the following closed-loop system:

$$\begin{cases} \dot{x}(t) = \sum_{i=1}^{4}\sum_{j=1}^{4} \mu_i^t \mu_j^r [\xi_{ij}(t) + \zeta_{ij}(t)], \\ y(t) = Cx(t) \end{cases} \tag{17}$$

for $t \in \mathcal{T}_n$, where $\mu_i^t \triangleq \mu_i\big(h(t)\big)$, $\mu_j^r \triangleq \mu_j\big(h(r_n h)\big)$, and

$$\begin{aligned} \xi_{ij}(t) &= A_i x(t) + \bar{\chi} B_{ui} K_j p(y(t)) + \sum_{m=1}^{l-1} \bar{\delta}_m^n B_{ui} K_j C \Pi_m^n(t) \\ &\quad + (1 - \sum_{m=1}^{l-1} \bar{\delta}_m^n) B_{ui} K_j C \Pi_l^n(t) + B_\omega \omega(t) \\ \zeta_{ij}(t) &= (\chi(t) - \bar{\chi}) B_{ui} K_j p(y(t)) \\ &\quad + \sum_{m=1}^{l-1} (\delta_m^n(t) - \bar{\delta}_m^n) B_{ui} K_j C \Pi_m^n(t) \\ &\quad + \sum_{m=1}^{l-1} (\bar{\delta}_m^n - \delta_m^n(t)) B_{ui} K_j C \Pi_l^n(t). \end{aligned}$$

The main objective of this paper is to develop a fuzzy OFC (14) together with the VPRS-based ETM, aiming to ensure H_∞ mean-square asymptotic stability (MSAS) of the T-S fuzzy power system considering multiple new energy power generations subject to random FDI attacks.

III. Co-Design of the LFC and the VPRS-Based ETM

Before the design of LFC and VPRS-based ETM for the power system in (17), we define the following definitions of symbols:

$$\begin{aligned} \phi_1(t) &= \mathfrak{C}_{m=1}^l\{x(t-\tau_m^n(t))\}, \phi_2(t) = \mathfrak{C}_{m=1}^l\{e_m^n(t)\}, \\ \phi(t) &= [x^T(t)\ \phi_1^T(t)\ x^T(t-\tau_M)\ \phi_2(t)\ \omega^T(t)\ f^T(y(t))]^T, \\ \mathfrak{I}_g &= [0_{7\times 7(g-1)}\ I_{7\times 7}\ 0_{7\times 7(2l+2-g)}\ 0_{7\times 1}\ 0_{7\times 2}], g \in \mathfrak{N}_{2l+2} \\ \mathfrak{I}_{g\omega} &= [0_{7\times 7(2l+2)}\ I_\omega\ 0_{7\times 2}], I_\omega^T = [1\ \mathfrak{C}_6^T\{0\}], \\ \mathfrak{I}_{gp} &= [0_{7\times 7(2l+2)}\ 0_{7\times 1}\ I_p], \\ I_p^T &= \begin{bmatrix} 1 & 0 & \mathfrak{C}_5^T\{0\} \\ 0 & 1 & \mathfrak{C}_5^T\{0\} \end{bmatrix}. \end{aligned}$$

Given the fuzzy output feedback controller gain K_j, $j \in \mathfrak{N}_4$, sufficient conditions of MSAS for the power system in (17) can be obtained in the following theorem.

Theorem 1: Consider the closed-loop power system in (17) with the VPRS-based ETM in (8). For given parameters κ_j, θ, $\bar{\chi}$, $\hat{\chi}$, l, controller gain K_j, matrix $\mathcal{M}$, and scalars $\bar{\delta}_m^1$, $\hat{\delta}_m^1$, if there exist symmetric matrices $P > 0$, $P_f > 0$, $Q > 0$, $R_\lambda > 0$, $\Xi > 0$, and Δ_i, and matrices U_λ with appropriate dimensions such that

$$\Omega_{ij} - \Delta_i < 0, \tag{18}$$

$$\Lambda_{ii} < 0, \tag{19}$$

$$\Lambda_{ij} + \Lambda_{ji} < 0,\ i < j \tag{20}$$

$$\mathscr{R}_\lambda^U > 0, \tag{21}$$

for $i,\ j \in \mathfrak{N}_4,\ m \in \mathfrak{N}_{l-1},\ n \in N,\ \lambda \in \mathfrak{N}_l$, where

$$\begin{aligned} \Omega_{ij} &= \mathfrak{S}\{\Omega_{ij}^1, *; \Sigma_{ij}, \Gamma\}, \\ \Omega_{ij}^1 &= \mathbf{He}\{\mathfrak{I}_1^T P \mathfrak{A}_{ij}\} + \mathfrak{T}\{\mathfrak{I}_1, Q\} - \mathfrak{T}\{\mathfrak{I}_{l+2}, Q\} \\ &\quad + \sum_{\lambda=1}^{l}\Big[- \mathfrak{T}\{\mathfrak{W}_\lambda, \mathscr{R}_\lambda^U\} - \mathfrak{T}\{C\mathfrak{I}_{l+2+\lambda}, \Xi\} \\ &\quad + \mathfrak{T}\{(C\mathfrak{I}_{\lambda+1} + C\mathfrak{I}_{l+2+\lambda}), \theta\Xi\}\Big] - \mathfrak{T}\{I_\omega^T \mathfrak{I}_{g\omega}, \epsilon^2 I_\epsilon\} \\ &\quad - \mathfrak{T}\{I_p^T \mathfrak{I}_{gp}, P_f\}, \\ \Sigma_{ij} &= \mathfrak{C}_{s=1}^4\{\mathcal{D}_{ij}^s\}, \mathcal{D}_{ij}^1 = \mathfrak{C}_{\lambda=1}^l\{\tau_M R_\lambda \mathfrak{A}_{ij}\}, \\ \mathcal{D}_{ij}^2 &= \mathfrak{C}_{\lambda=1}^l\Big\{\mathfrak{C}_{m=1}^{l-1}\{\hat{\delta}_m^n \tau_M R_\lambda B_{ui} K_j C[\mathfrak{I}_{m+1} + \mathfrak{I}_{l+2+m} \\ &\quad - \mathfrak{I}_{l+1} - \mathfrak{I}_{2l+2}]\}\Big\}, \\ \mathcal{D}_{ij}^3 &= \mathfrak{C}_{\lambda=1}^l\{\hat{\chi}\tau_M R_\lambda B_{ui} K_j I_p^T \mathfrak{I}_{gp}\}, \\ \mathcal{D}_{ij}^4 &= \mathfrak{C}\{C, P_f \mathcal{M} C\}, \\ \Gamma &= \mathbf{diag}\Big\{\mathbf{diag}_{\lambda=1}^l\{-R_\lambda\}, \mathbf{diag}_{\lambda=1}^l\big\{\mathbf{diag}_{l-1}\{-R_\lambda\}\big\}, \\ &\quad \mathbf{diag}_{\lambda=1}^l\{-R_\lambda\}, -I, -P_f\Big\}, \\ \mathfrak{A}_{ij} &= A_i\mathfrak{I}_1 + \sum_{m=1}^{l-1} \bar{\delta}_m^n B_{ui} K_j C[\mathfrak{I}_{m+1} + \mathfrak{I}_{l+2+m}] \\ &\quad + (1 - \sum_{m=1}^{l-1} \bar{\delta}_m^n) B_{ui} K_j C[\mathfrak{I}_{l+1} + \mathfrak{I}_{2l+2}] \\ &\quad + B_\omega I_\omega^T \mathfrak{I}_{g\omega} + \bar{\chi} B_{ui} K_j I_p^T \mathfrak{I}_{gp}, \\ \mathfrak{W}_\lambda &= \mathfrak{C}_{s=1}^2\{\mathfrak{W}_{\lambda s}\},\ \mathfrak{W}_{\lambda 1} = \mathfrak{I}_1 - \mathfrak{I}_{\lambda+1}, \\ \mathfrak{W}_{\lambda 2} &= \mathfrak{I}_{\lambda+1} - \mathfrak{I}_{l+2}, \\ \mathscr{R}_\lambda^U &= \mathfrak{S}\{R_\lambda, *; U_\lambda, R_\lambda\}. \end{aligned}$$

Then, the closed-loop power system (17) is MSAS with H_∞ level ϵ.

Proof: Construct the following Lyapunov functional:

$$V(t) = V_1(t) + V_2(t) + V_3(t), \tag{22}$$

where $V_1(t) = \mathfrak{T}\{x(t), P\}$, $V_2(t) = \int_{t-\tau_M}^t \mathfrak{T}\{x(s), Q\}ds$, and $V_3(t) = \sum_{\lambda=1}^l \tau_M \int_{t-\tau_M}^t (s-t+\tau_M)\mathfrak{T}\{\dot{x}(s), R_\lambda\}ds$.

Taking the derivative of $V(t)$ along the trajectory (17) and taking its expectation yield that

$$\mathbb{E}\{\dot{V}_1(t)\} = \mathbb{E}\Big\{\sum_{i,j=1}^{4} \mu_i^t \mu_j^r \mathfrak{T}\big\{\phi(t), \mathbf{He}\{\mathfrak{I}_1^T P \mathfrak{A}_{ij}\}\big\}\Big\}, \tag{23}$$

$$\mathbb{E}\{\dot{V}_2(t)\} = \mathfrak{T}\Big\{\phi(t), \big(\mathfrak{T}\{\mathfrak{I}_1, Q\} - \mathfrak{T}\{\mathfrak{I}_{l+2}, Q\}\big)\Big\}, \tag{24}$$

and

$$\begin{aligned} \mathbb{E}\{\dot{V}_3(t)\} &= \sum_{\lambda=1}^{l} \mathbb{E}\Big\{\tau_M^2 \mathfrak{T}\{\dot{x}(t), R_\lambda\} \\ &\quad - \tau_M \int_{t-\tau_M}^t \mathfrak{T}\{\dot{x}(s), R_\lambda\}ds\Big\}. \end{aligned} \tag{25}$$

Notice that

$$\begin{aligned}&\mathbb{E}\{\tau_M^2\mathfrak{T}\{\dot{x}(t),R_\lambda\}\}\\&=\sum_{i,j=1}^{4}\mu_i^t\mu_j^r\mathbb{E}\Big\{\mathfrak{T}\{\phi(t),\mathfrak{T}\{\tau_M R_\lambda\mathfrak{A}_{ij},R_\lambda^{-1}\}\}\\&+\mathfrak{T}\Big\{\phi(t),\Big[\sum_{m=1}^{l-1}\mathfrak{T}\{\hat{\delta}_m^n\tau_M R_\lambda B_{ui}K_jC[\mathfrak{I}_{m+1}\\&+\mathfrak{I}_{l+2+m}-\mathfrak{I}_{l+1}-\mathfrak{I}_{2l+2}],R_\lambda^{-1}\}\\&+\mathfrak{T}\{\hat{\chi}\tau_M R_\lambda B_{ui}K_jI_p^T\mathfrak{I}_{gp},R_\lambda^{-1}\}\Big]\Big\}\Big\},\end{aligned}\tag{26}$$

and

$$\begin{aligned}&\mathbb{E}\Big\{-\tau_M\int_{t-\tau_M}^{t}\mathfrak{T}\{\dot{x}(s),R_\lambda\}ds\Big\}\\&=-\tau_M\int_{t-\tau_M}^{t-\tau_\lambda^n(t)}\mathfrak{T}\{\dot{x}(s),R_\lambda\}ds-\tau_M\int_{t-\tau_\lambda^n(t)}^{t}\mathfrak{T}\{\dot{x}(s),R_\lambda\}ds\\&\le-\mathfrak{T}\{\phi(t),\mathfrak{T}\{\mathfrak{W}_\lambda,\mathscr{R}_\lambda^U\}\}.\end{aligned}$$

Considering VPRS-based ETM in (8) yields that

$$\begin{aligned}\sum_{\lambda=1}^{l}\Big\{&\mathfrak{T}\{\phi(t),[\mathfrak{T}\{(C\mathfrak{I}_{\lambda+1}+C\mathfrak{I}_{l+2+\lambda}),\theta\Xi\}\\&-\mathfrak{T}\{C\mathfrak{I}_{l+2+\lambda},\Xi\}]\}\Big\}\ge 0.\end{aligned}\tag{27}$$

In addition, from the FDI attack restriction represented in (15), for $P_f>0$, we have

$$\mathfrak{T}\{\phi(t),\mathfrak{T}\{I_p^T\mathfrak{I}_{gp},P_f\}\}-\mathfrak{T}\{\phi(t),\mathfrak{T}\{P_f\mathcal{M}C\mathfrak{I}_1,P_f^{-1}\}\}\le 0.\tag{28}$$

Combining (23)-(28), we obtain

$$\begin{aligned}\mathbb{E}\{\dot{V}(t)\}&=\mathbb{E}\{\dot{V}_1(t)\}+\mathbb{E}\{\dot{V}_2(t)\}+\mathbb{E}\{\dot{V}_3(t)\}\\&\le\sum_{i,j=1}^{4}\mu_i^t\mu_j^r\mathfrak{T}\Big\{\phi(t),\Big\{\mathbf{He}\{\mathfrak{I}_1^TP\mathfrak{A}_{ij}\}+\mathfrak{T}\{\mathfrak{I}_1,Q\}\\&-\mathfrak{T}\{\mathfrak{I}_{l+2},Q\}+\sum_{\lambda=1}^{l}\Big[\mathfrak{T}\{\tau_M R_\lambda\mathfrak{A}_{ij},R_\lambda^{-1}\}\\&+\sum_{m=1}^{l-1}\mathfrak{T}\{\hat{\delta}_m^n\tau_M R_\lambda B_{ui}K_jC[\mathfrak{I}_{m+1}+\mathfrak{I}_{l+2+m}-\mathfrak{I}_{l+1}\\&-\mathfrak{I}_{2l+2}],R_\lambda^{-1}\}+\mathfrak{T}\{\hat{\chi}\tau_M R_\lambda B_{ui}K_jI_p^T\mathfrak{I}_{gp},R_\lambda^{-1}\}\\&-\mathfrak{T}\{\mathfrak{W}_\lambda,\mathscr{R}_\lambda^U\}-\mathfrak{T}\{C\mathfrak{I}_{l+2+\lambda},\Xi\}\\&+\mathfrak{T}\{(C\mathfrak{I}_{\lambda+1}+C\mathfrak{I}_{l+2+\lambda}),\theta\Xi\}\Big]+\mathfrak{T}\{C\mathfrak{I}_1,I_y\}\\&-\mathfrak{T}\{C\mathfrak{I}_1,I_y\}-\mathfrak{T}\{I_\omega^T\mathfrak{I}_{g\omega},\epsilon^2I_\epsilon\}\\&+\mathfrak{T}\{I_\omega^T\mathfrak{I}_{g\omega},\epsilon^2I_\epsilon\}+\mathfrak{T}\{P_f\mathcal{M}C\mathfrak{I}_1,P_f^{-1}\}\\&-\mathfrak{T}\{I_p^T\mathfrak{I}_{gp},P_f\}\Big\}\Big\}\\&=\mathbb{E}\Big\{\sum_{i,j=1}^{4}\mu_i^t\mu_j^r\mathfrak{T}\{\phi(t),\Omega_{ij}\}\Big\}\\&-\mathfrak{T}\{\phi(t),[\mathfrak{T}\{C\mathfrak{I}_1,I_y\}-\mathfrak{T}\{I_\omega^T\mathfrak{I}_{g\omega},\epsilon^2I_\epsilon\}]\}.\end{aligned}\tag{29}$$

Due to $\sum_{i=1}^{4}\mu_i^t=\sum_{j=1}^{4}\mu_j^r=1$, it has

$$\mathbb{E}\Big\{\sum_{i=1}^{4}\mu_i^t\sum_{j=1}^{4}(\mu_j^t-\mu_j^r)\mathfrak{T}\{\phi(t),\Delta_i\}\Big\}=0.\tag{30}$$

Thus, (29) can be represented as follows

$$\begin{aligned}\mathbb{E}\{\dot{V}(t)\}&\le\mathbb{E}\Big\{\sum_{i,j=1}^{4}\mu_i^t\mu_j^r\mathfrak{T}\{\phi(t),\Omega_{ij}\}\Big\}\\&-\mathfrak{T}\{\phi(t),[\mathfrak{T}\{C\mathfrak{I}_1,I_y\}-\mathfrak{T}\{I_\omega^T\mathfrak{I}_{g\omega},\epsilon^2I_\epsilon\}]\}\\&\le\mathbb{E}\Big\{\sum_{i,j=1}^{4}\mu_i^t\mu_j^r\mathfrak{T}\{\phi(t),\Omega_{ij}\}\\&+\sum_{i,j=1}^{4}\mu_i^t(\mu_j^t-\mu_j^r)\mathfrak{T}\{\phi(t),\Delta_i\}\Big\}\\&-\mathfrak{T}\{\phi(t),[\mathfrak{T}\{C\mathfrak{I}_1,I_y\}-\mathfrak{T}\{I_\omega^T\mathfrak{I}_{g\omega},\epsilon^2I_\epsilon\}]\}\\&=\mathbb{E}\Big\{\sum_{i,j=1}^{4}\mu_i^t\mu_j^r\mathfrak{T}\{\phi(t),(\Omega_{ij}-\Delta_i)\}\\&+\sum_{i,j=1}^{4}\mu_i^t\mu_j^t\mathfrak{T}\{\phi(t),\Delta_i\}\Big\}\\&-\mathfrak{T}\{\phi(t),[\mathfrak{T}\{C\mathfrak{I}_1,I_y\}-\mathfrak{T}\{I_\omega^T\mathfrak{I}_{g\omega},\epsilon^2I_\epsilon\}]\}.\end{aligned}\tag{31}$$

By recalling (13) and (18), (31) can be rewritten as

$$\begin{aligned}\mathbb{E}\{\dot{V}(t)\}&\le\mathbb{E}\Big\{\sum_{i,j=1}^{4}\mu_i^t\mu_j^r\mathfrak{T}\{\phi(t),\Omega_{ij}\}\Big\}\\&-\mathfrak{T}\{\phi(t),[\mathfrak{T}\{C\mathfrak{I}_1,I_y\}-\mathfrak{T}\{I_\omega^T\mathfrak{I}_{g\omega},\epsilon^2I_\epsilon\}]\}\\&\le\mathbb{E}\Big\{\sum_{i,j=1}^{4}\mu_i^t\mu_j^t\mathfrak{T}\{\phi(t),\kappa_j(\Omega_{ij}-\Delta_i)\}\\&+\sum_{i,j=1}^{4}\mu_i^t\mu_j^t\mathfrak{T}\{\phi(t),\Delta_i\}\Big\}\\&-\mathfrak{T}\{\phi(t),[\mathfrak{T}\{C\mathfrak{I}_1,I_y\}-\mathfrak{T}\{I_\omega^T\mathfrak{I}_{g\omega},\epsilon^2I_\epsilon\}]\}\\&\le\mathbb{E}\Big\{\sum_{i,j=1}^{4}\mu_i^t\mu_j^t\mathfrak{T}\{\phi(t),\Lambda_{ii}\}\\&+\sum_{i}^{4}\sum_{i<j}\mu_i^t\mu_j^t\mathfrak{T}\{\phi(t),(\Lambda_{ij}+\Lambda_{ji})\}\Big\}\\&-\mathfrak{T}\{\phi(t),[\mathfrak{T}\{C\mathfrak{I}_1,I_y\}-\mathfrak{T}\{I_\omega^T\mathfrak{I}_{g\omega},\epsilon^2I_\epsilon\}]\}\end{aligned}\tag{32}$$

where $\Lambda_{ij}=\kappa_j(\Omega_{ij}-\Delta_i)+\Delta_i$.

Then, we can conclude that $\mathbb{E}\{\dot{V}(t)\}<-\mathfrak{T}\{y(t),I_y\}<0$ for $\omega(t)=0$, if the LMIs (18)-(21) are hold, while for zero initial condition, it has $\mathfrak{T}\{y(t),I_y\}\le\mathfrak{T}\{\omega(t),\epsilon^2I_\epsilon\}$ for $\omega(t)\ne 0$. That is, the system (17) is MSAS with H_∞ norm bound ϵ. The proof is completed. ■

Subsequently, the controller gains K_j for $j\in\mathfrak{N}_4$ and the weight matrix Ξ of the VPRS-based ETM will be formulated in the light of Theorem 1.

Theorem 2: Consider the closed-loop power system in (17) with the VPRS-based ETM in (8). For given scalars κ_j, l, θ, $\bar{\chi}$, $\hat{\chi}$, $\bar{\delta}_m^n$, $\hat{\delta}_m^n$, γ, matrix $\mathcal{M}$, and a small enough scalar $\wp$,

if there exist symmetric matrices $X > 0$, $\tilde{Q} > 0$, $\tilde{R}_\lambda > 0$, $\tilde{\Xi} > 0$, and $\tilde{\Delta}_i$, and matrices $\tilde{U}_{\lambda 1}$, $\tilde{U}_{\lambda 2}$, $\tilde{U}_{\lambda 3}$ such that

$$\tilde{\Omega}_{ij} < 0, \tag{33}$$
$$\tilde{\Lambda}_{ii} < 0 \tag{34}$$
$$\tilde{\Lambda}_{ij} + \tilde{\Lambda}_{ji} < 0, \ i < j \tag{35}$$
$$\tilde{\mathscr{R}}_\lambda^U > 0, \tag{36}$$
$$\mathcal{X}_f^C < 0 \tag{37}$$

for $i, j \in \mathfrak{N}_4$, $\lambda \in \mathfrak{N}_l$, and $m \in \mathfrak{N}_{l-1}$, where

$$\begin{aligned}
\tilde{\Omega}_{ij} &= \mathfrak{S}\{\tilde{\Omega}_{ij}^1, *; \tilde{\Sigma}_{ij}, \tilde{\Gamma}\},\\
\tilde{\Omega}_{ij}^1 &= \mathbf{He}\{\mathfrak{I}_1^T \tilde{\mathfrak{A}}_{ij}\} + \mathfrak{T}\{\mathfrak{I}_1, \tilde{Q}\} - \mathfrak{T}\{\mathfrak{I}_{l+2}, \tilde{Q}\}\\
&\quad + \sum_{\lambda=1}^{l}\Big[-\mathfrak{T}\{\mathfrak{W}_\lambda, \tilde{\mathscr{R}}_\lambda^U\} - \mathfrak{T}\{\mathfrak{I}_{l+2+\lambda}, \tilde{\Xi}\}\\
&\quad + \mathfrak{T}\{(\mathfrak{I}_{\lambda+1} + \mathfrak{I}_{l+2+\lambda}), \theta\tilde{\Xi}\}\Big]\\
&\quad - \mathfrak{T}\{I_\omega^T \mathfrak{I}_{g\omega}, \epsilon^2 I_\epsilon\} - \mathfrak{T}\{I_p^T \mathfrak{I}_{gp}, X_f\},\\
\tilde{\mathscr{R}}_\lambda^U &= \mathfrak{S}\{\tilde{R}_\lambda, *; \tilde{U}_\lambda, \tilde{R}_\lambda\},\\
\tilde{\Lambda}_{ij} &= \kappa_j(\tilde{\Omega}_{ij} - \tilde{\Delta}_i) + \tilde{\Delta}_i,\\
\mathcal{X}_f^C &= \mathfrak{S}\{-\wp I, \ *; \ (X_f C - CX), \ -I\},\\
\tilde{\mathfrak{A}} &= A_i X \mathfrak{I}_1 + \sum_{m=1}^{l-1} \bar{\delta}_m^n B_{ui} H_j C[\mathfrak{I}_{m+1} + \mathfrak{I}_{l+2+m}],\\
&\quad + (1 - \sum_{m=1}^{l-1} \bar{\delta}_m^n) B_{ui} H_j C[\mathfrak{I}_{l+1} + \mathfrak{I}_{2l+2}]\\
&\quad + B_\omega I_\omega^T \mathfrak{I}_{g\omega} + \bar{\chi} B_{ui} H_j I_p^T \mathfrak{I}_{gp},\\
\tilde{\Sigma}_{ij} &= \mathfrak{C}_{s=1}^4\{\tilde{\mathcal{D}}_{ij}^s\}, \quad \tilde{\mathcal{D}}_{ij}^1 = \mathfrak{C}_l\{\tau_M \tilde{\mathfrak{A}}_{ij}\},\\
\tilde{\mathcal{D}}_{ij}^2 &= \mathfrak{C}_l\Big\{\mathfrak{C}_{m=1}^{l-1}\{\hat{\delta}_m^n \tau_M B_{ui} H_j C[\mathfrak{I}_{m+1} + \mathfrak{I}_{l+2+m} - \mathfrak{I}_{l+1}\\
&\quad - \mathfrak{I}_{2l+2}]\}\Big\},\\
\tilde{\mathcal{D}}_{ij}^3 &= \mathfrak{C}_{\lambda=1}^l\{\hat{\chi}\tau_M B_{ui} H_j I_p^T \mathfrak{I}_{gp}\},\\
\tilde{\mathcal{D}}_{ij}^4 &= \mathfrak{C}\{X_f C, \mathcal{M} X_f C\},\\
\tilde{\Gamma} &= \mathbf{diag}\Big\{\mathbf{diag}_{\lambda=1}^l\{\urcorner\}, \mathbf{diag}_{\lambda=1}^l\{\mathbf{diag}_{l-1}\{\urcorner\}\},\\
&\quad \mathbf{diag}_{\lambda=1}^l\{\urcorner\}, -I, -X_f\Big\},\\
\urcorner &= \gamma^2 \tilde{R}_\lambda - 2\gamma X.
\end{aligned}$$

Then, the system (17) under the control law in (16) with $K_j = H_j X_f^{-1}$, $j \in \mathfrak{N}_4$ is MSAS with H_∞ norm bound ϵ. Moreover, the weight matrix of the VPRS-based ETM in (8) is given by $\Xi = CX^{-1}\tilde{\Xi}X^{-1}C^T$.

Proof: Define $X = P^{-1}$, $X_f = P_f^{-1}$, $\tilde{Q} = \mathfrak{T}\{X, Q\}$, $\tilde{R}_\lambda = \mathfrak{T}\{X, R_\lambda\}$, $\tilde{\Xi} = \mathfrak{T}\{X, C^T \Xi C\}$, and $\tilde{\Delta}_i = \mathfrak{T}\{X, \Delta_i\}$, $\tilde{U}_\lambda = \mathfrak{T}\{X, U_\lambda\}$, $\tilde{\mathscr{R}}_\lambda^U = \mathfrak{T}\{\mathbf{diag}_2\{X\}, \mathscr{R}_\lambda^U\}$, and $\aleph = \mathbf{diag}\{\mathfrak{I}_1, I, X_f, \mathfrak{I}_2, \mathfrak{I}_3, \mathfrak{I}_4, I, X_f\}$, where $\mathfrak{I}_1 = \mathbf{diag}_{2l+2}\{X\}$, $\mathfrak{I}_2 = \mathbf{diag}_{\lambda=1}^l\{R_\lambda^{-1}\}$, $\mathfrak{I}_3 = \mathbf{diag}_{\lambda=1}^l\{\mathbf{diag}_{l-1}\{R_\lambda^{-1}\}\}$, $\mathfrak{I}_4 = \mathbf{diag}_{\lambda=1}^l\{R_\lambda^{-1}\}$.

Inspired by the method in [12] for dealing with the nonlinear item $K_j CX$, we assume $(X_f C - CX)^T (X_f C - CX) = 0$ which is guaranteed by (37). Substituting $K_j CX$ and CX with $H_j C$ and $X_f C$, respectively, then the (33) can be obtained by pre- and post-multiplying (18) with $\aleph$ and considering the above substitution, and (34)-(36) are also derived by using the same method. Due to the fact $CC^T = \mathbf{diag}\{1, 1\}$, the weight matrix of the VPRS-based ETM can be calculated by $\Xi = CX^{-1}\tilde{\Xi}X^{-1}C^T$. The proof is completed. ■

In Section II-B, the RHOC strategy is presented, where the transmission probability $\bar{\delta}_m^n$ is updated using data from various groups. This update results in alterations to the control gains and the weight matrix of the VPRS-based ETM, ultimately optimizing control performance. Next, we will present an algorithm that effectively implements this strategy.

Algorithm 1 The RHOC Strategy

Input: Parameters needed in Theorem 2
Output: K_j^n, Ξ^n, and $\bar{\delta}_m^n$
Initialize $\delta_m^1 = 1/l, \forall m \in \mathfrak{N}_l$;
Solve for K_j^1 and Ξ^1 according to Theorem 2;
for $n = 2 : N$ **do**
  Compute $\bar{\delta}_m^n, \forall m \in \mathfrak{N}_l$ using (7);
  if $\|\bar{\delta}_m^n - \bar{\delta}_m^{n-1}\| < \varepsilon, \forall m \in \mathfrak{N}_l$ **then**
    Output $K_j^n = K_j^{n-1}, \forall j \in \mathfrak{N}_4$, $\Xi^n = \Xi^{n-1}$, and $\bar{\delta}_m^n = \bar{\delta}_m^{n-1}, \forall m \in \mathfrak{N}_l$;
  end
  else
    Solve K_j^n, Ξ^n, and $\bar{\delta}_m^n$ according to Theorem 2;
    if *no solution to Theorem 2* **then**
      Output $K_j^n = K_j^{n-1}, \forall j \in \mathfrak{N}_4$, $\Xi^n = \Xi^{n-1}$, and $\bar{\delta}_m^n = \bar{\delta}_m^{n-1}, \forall m \in \mathfrak{N}_l$;
    end
    else
      Output K_j^n, Ξ^n, and $\bar{\delta}_m^n$;
    end
  end
end

Remark 4: In Algorithm 1, the LMIs (33)-(37) are computed only when the condition $\|\bar{\delta}_m^n - \bar{\delta}_m^{n-1}\| < \varepsilon$ violated, thereby saving the computational resources.

IV. Application Example

In this section, we employ a power system integrating with EVs and PPGSs to validate the effectiveness of the proposed VPRS-based ETM under scenarios involving random FDI attacks. The parameters for the power system's dynamic model (1) are referred from both [1] and [29].

$$D = 0.0083;\ M = 0.1667;\ R_g = 2.4;\ T_g = 0.08;\ T_t = 0.3;$$
$$\rho_e = 0.4167;\ T_e = 1;\ b = 0.425;\ \alpha_g = 0.8;\ \alpha_e = 0.2;$$
$$T_{p1} = 99.5;\ T_{p2} = -50;\ T_{p3} = 0.5;\ \alpha_p = 0.3,$$

and $h_1(t) = 1 + \frac{1}{5}sin(t)$ and $h_2(t) = -18 + 2cos(t)$, respectively.

Assume the FDI attacks are restrained by $p(y(t)) = [-\tanh(0.2y_1); -\tanh(0.1y_2)]$; the initial state is $x(0) = [0.1; 0.01; 0.04; 0.02; 0.01; 0.01; 0.12]$; and the external disturbance is given by $\omega(t) = 0.1e^{-t}$.

Moreover, the inputs in Algorithm 1 are given by $\kappa_1 = 0.9$, $\kappa_2 = 0.8$, $\kappa_3 = 0.9$, $\kappa_1 = 0.8$, $\epsilon = 10$, $\gamma = 0.63$, $\theta = 0.1$,

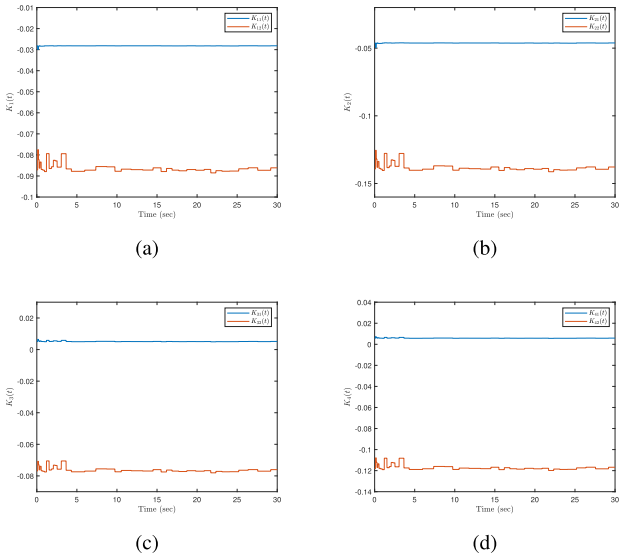

Fig. 3. Controller gains with $l = 3$.

$\bar{\delta}_1^1 = \bar{\delta}_2^1 = \bar{\delta}_3^1 = 1/3$, $\bar{\chi} = 0.2$, and $\wp = 0.01$. Applying Theorem 2 with $l = 3$ and Algorithm 1 and sampling period $h = 0.01$, we can obtain the feedback gains and weight matrices of VPRS-based ETM as follows:

$$\begin{bmatrix} K_1^1 = [-0.0282 \ \ -0.0871]; & K_2^1 = [-0.0462 \ \ -0.1393] \\ K_3^1 = [0.0050 \ \ -0.0769]; & K_4^1 = [0.0058 \ \ -0.1180] \end{bmatrix},$$
$$\begin{bmatrix} K_1^2 = [-0.0299 \ \ -0.0775]; & K_2^2 = [-0.0495 \ \ -0.1255] \\ K_3^2 = [0.0065 \ \ -0.0708]; & K_4^2 = [0.0072 \ \ -0.1079] \end{bmatrix},$$
$$\begin{bmatrix} K_1^3 = [-0.0283 \ \ -0.0823]; & K_2^3 = [-0.0464 \ \ -0.1320] \\ K_3^3 = [0.0056 \ \ -0.0730]; & K_4^3 = [0.0063 \ \ -0.1121] \end{bmatrix},$$
$$\vdots$$

The variations in controller gains K_j^n are depicted in Fig. 3, illustrating their dependency on group n. Under these time-varying gains, the frequency responses of the power systems are shown in Fig. 4 with the blue dotted line. It is observed that, despite external disturbances and the varying gains of EVs and PPGSs, the LFC power system is MSAS, ultimately converging to the equilibrium point around 15 seconds.

By combining Figs. 3 and 4, it is evident that the controller gains exhibit big variation during periods of substantial system state changes. This adjustment enables the system to better adapt to disturbances, thereby enhancing the overall control effectiveness in LFC power systems. This illustrates the RHOC strategy can makes up for the adverse effects caused by discarding a large number of triggered packets.

In addition, for the purpose of saving network resource, our proposed VPRS-based ETM is utilized. Under this communication strategy, the release instants and interval (RIIs) is depicted in Fig. 5(a), from which one can see that, during 0-30s, only 14 FRPs (that is 0.47% sampled data packets) are transmitted over the network, thereby mitigating the burden of network bandwidth.

To illustrate the advantages of our proposed methods, we set $l = 1$, as stated in Remark 2, the proposed VPRS-based ETM turns to be a conventional ETM as in [20]. Based on

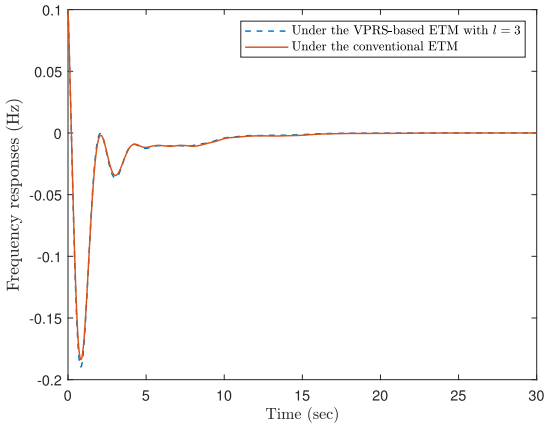

Fig. 4. Frequency responses.

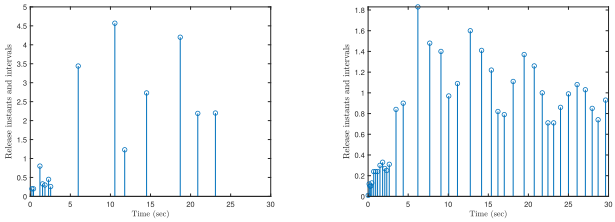

Fig. 5. RIIs. (a) under VPRS-based ETM with $l = 3$. (b) under the conventional ETM.

Theorem 2, controller gains can be calculated as

$$K_1 = [-0.0234 \ \ -0.0772]; \ K_2 = [-0.0383 \ \ -0.1220];$$
$$K_3 = [0.0064 \ \ -0.0713]; \quad K_4 = [0.0087 \ \ -0.1073].$$

Figs. 4 and 5(b) display the frequency responses of the fuzzy power system in (17) and RIIs, respectively. A comparison in Fig. 4 demonstrates the LFC performance of the power system under these two communication mechanisms is similar. While the number of APRs reaches 38 under the conventional ETM, it is about 2.7 times compared to our proposed VPRS-based ETM. This significant difference indicates that our method can significantly save network resources.

V. Conclusion

In this study, an innovative RHOC strategy has been developed to effectively tackle the LFC challenges in power systems incorporating EVs and PPGSs. A T-S fuzzy model is established to address the perturbation and nonlinear features resulting from the integration of EVs and PPGSs within real-world power systems. The RHOC strategy, coupled with a novel VPRS-based ETM, is introduced to balance LFC performance with limited communication resources. Sufficient conditions are derived to ensure the MSAS of power systems with limited utilization of communication resources. Simulation results showcase a remarkable conservation of network resources and heightened robustness in power systems, even when subjected to unreliable networks. Future work will extend the proposed RHOC algorithm to tackle the challenges associated with multi-area LFC systems.

REFERENCES

[1] X. Tang, Y. Li, M. Yang, Y. Wu, and Y. Wen, "Adaptive event-triggered model predictive load frequency control for power systems," *IEEE Trans. Power Syst.*, vol. 38, no. 5, pp. 4003–4014, Sep. 2023.

[2] S. Tripathi, V. P. Singh, N. Kishor, and A. S. Pandey, "Load frequency control of power system considering electric vehicles' aggregator with communication delay," *Int. J. Electr. Power Energy Syst.*, vol. 145, Feb. 2023, Art. no. 108697.

[3] D. K. Panda, S. Das, and S. Townley, "Toward a more renewable energy-based LFC under random packet transmissions and delays with stochastic generation and demand," *IEEE Trans. Autom. Sci. Eng.*, vol. 19, no. 2, pp. 1217–1232, Apr. 2022.

[4] X. Li and D. Ye, "Security-based event-triggered fuzzy control for multiarea power systems under cross-layer DoS attacks," *IEEE Trans. Circuits Syst. I, Reg. Papers*, vol. 70, no. 7, pp. 2995–3004, Jul. 2023.

[5] X.-C. Shangguan, Y. He, C.-K. Zhang, L. Jiang, and M. Wu, "Adjustable event-triggered load frequency control of power systems using control-performance-standard-based fuzzy logic," *IEEE Trans. Fuzzy Syst.*, vol. 30, no. 8, pp. 3297–3311, Aug. 2022.

[6] V. Gholamrezaie, M. G. Dozein, H. Monsef, and B. Wu, "An optimal frequency control method through a dynamic load frequency control (LFC) model incorporating wind farm," *IEEE Syst. J.*, vol. 12, no. 1, pp. 392–401, Mar. 2018.

[7] G. Zhang, J. Li, Y. Xing, O. Bamisile, and Q. Huang, "Data-driven load frequency cooperative control for multi-area power system integrated with VSCs and EV aggregators under cyber-attacks," *ISA Trans.*, vol. 143, pp. 440–457, Dec. 2023.

[8] M. Zhang, S. Dong, P. Shi, G. Chen, and X. Guan, "Distributed observer-based event-triggered load frequency control of multiarea power systems under cyber attacks," *IEEE Trans. Autom. Sci. Eng.*, vol. 20, no. 4, pp. 2435–2444, Oct. 2023.

[9] V. Kapil and S. Prasad, "Event-triggered intelligent control scheme for data integrity attack mitigation in multi-area power grids," *IEEE Trans. Power Syst.*, early access, May 9, 2024, doi: 10.1109/TPWRS.2024.3398693.

[10] Z. Zhang, J. Hu, J. Lu, J. Cao, and J. Yu, "False data injection attacks on LFC systems: An AI-based detection and countermeasure strategy," *IEEE Trans. Circuits Syst. I, Reg. Papers*, vol. 71, no. 5, pp. 1969–1977, May 2024.

[11] H. Wang and Z. S. Li, "Multi-area load frequency control in power system integrated with wind farms using fuzzy generalized predictive control method," *IEEE Trans. Rel.*, vol. 72, no. 2, pp. 737–747, Jun. 2023.

[12] C. Peng, J. Zhang, and H. Yan, "Adaptive event-triggering H_∞ load frequency control for network-based power systems," *IEEE Trans. Ind. Electron.*, vol. 65, no. 2, pp. 1685–1694, Feb. 2018.

[13] S. Yan, Z. Gu, J. H. Park, and X. Xie, "Sampled memory-event-triggered fuzzy load frequency control for wind power systems subject to outliers and transmission delays," *IEEE Trans. Cybern.*, vol. 53, no. 6, pp. 4043–4053, Dec. 2023.

[14] T. N. Pham, S. Nahavandi, L. V. Hien, H. Trinh, and K. P. Wong, "Static output feedback frequency stabilization of time-delay power systems with coordinated electric vehicles state of charge control," *IEEE Trans. Power Syst.*, vol. 32, no. 5, pp. 3862–3874, Sep. 2017.

[15] X.-G. Guo, D.-Y. Zhang, J.-L. Wang, J. H. Park, and L. Guo, "Observer-based event-triggered composite anti-disturbance control for multi-agent systems under multiple disturbances and stochastic FDIAs," *IEEE Trans. Autom. Sci. Eng.*, vol. 20, no. 1, pp. 528–540, Jan. 2023.

[16] F. Yang, X. Xie, Q. Sun, and D. Yue, "FDI attack estimation and event-triggered resilient control of DC microgrids under hybrid attacks," *IEEE Trans. Smart Grid*, vol. 15, no. 4, pp. 4207–4216, Jul. 2024.

[17] Q. Zhong, J. Yang, K. Shi, S. Zhong, Z. Li, and M. A. Sotelo, "Event-triggered H_∞ load frequency control for multi-area nonlinear power systems based on non-fragile proportional integral control strategy," *IEEE Trans. Intell. Transp. Syst.*, vol. 23, no. 8, pp. 12191–12201, Aug. 2022.

[18] G. Zhao, H. Cui, and C. Hua, "Hybrid event-triggered bipartite consensus control of multiagent systems and application to satellite formation," *IEEE Trans. Autom. Sci. Eng.*, vol. 20, no. 3, pp. 1760–1771, Jul. 2023.

[19] X. Liu et al., "Event-triggering load frequency control for multi-area power system based on random dynamic triggering mechanism and two-side closed functional," *ISA Trans.*, vol. 133, pp. 193–204, Feb. 2023.

[20] D. Yue, E. Tian, and Q.-L. Han, "A delay system method for designing event-triggered controllers of networked control systems," *IEEE Trans. Autom. Control*, vol. 58, no. 2, pp. 475–481, Feb. 2013.

[21] X. H. Li, C. K. Ahn, W. D. Zhang, and P. Shi, "Asynchronous event-triggered-based control for stochastic networked Markovian jump systems with FDI attacks," *IEEE Trans. Syst., Man, Cybern., Syst.*, vol. 53, no. 9, pp. 5955–5967, Sep. 2023.

[22] Y. Liu, Y. Chen, and M. Li, "Event-based model predictive damping control for power systems with cyber-attacks," *ISA Trans.*, vol. 136, pp. 687–700, May 2023.

[23] Y. Wang, W. Yan, H. Zhang, and X. Xie, "Observer-based dynamic event-triggered H_∞ LFC for power systems under actuator saturation and deception attack," *Appl. Math. Comput.*, vol. 420, May 2022, Art. no. 126896.

[24] Y. Wang, Z. Wang, J. Gan, H. Zhang, and R. Wang, "Switched observer-based adaptive event-triggered load frequency control for networked power systems under aperiodic DoS attacks," *IEEE Trans. Smart Grid*, vol. 14, no. 6, pp. 4816–4826, Nov. 2023.

[25] X. Liu, K. Shi, H. Yan, J. Cheng, and S. Wen, "Integral-based event-triggering switched LFC scheme for power system under deception attack," *Expert Syst. Appl.*, vol. 234, Dec. 2023, Art. no. 121075.

[26] Z. Gu, X. Huang, X. Sun, X. Xie, and J. H. Park, "Memory-event-triggered tracking control for intelligent vehicle transportation systems: A leader-following approach," *IEEE Trans. Intell. Transp. Syst.*, vol. 25, no. 5, pp. 4021–4031, May 2024.

[27] X. Liu, K. Shi, J. Cheng, S. Wen, and Y. Liu, "Adaptive memory-based event-triggering resilient LFC for power system under DoS attack," *Appl. Math. Comput.*, vol. 451, Aug. 2023, Art. no. 128041.

[28] L. Li, Y. Zhang, and T. Li, "Memory-based event-triggered output regulation for networked switched systems with unstable switching dynamics," *IEEE Trans. Cybern.*, vol. 52, no. 11, pp. 12429–12439, Nov. 2022.

[29] E. Tian and C. Peng, "Memory-based event-triggering H_∞ load frequency control for power systems under deception attacks," *IEEE Trans. Cybern.*, vol. 50, no. 11, pp. 4610–4618, Nov. 2020.

[30] M. I. Ibraheem, M. Edrisi, H. H. Alhelou, M. Gholipour, and A. Al-Hinai, "A sophisticated slide mode controller of microgrid system load frequency control under false data injection attack and actuator time delay," *IEEE Trans. Ind. Appl.*, vol. 60, no. 2, pp. 2117–2126, Mar. 2024.

[31] G. Zhang, J. Li, O. Bamisile, Y. Xing, D. Cai, and Q. Huang, "An H_∞ load frequency control scheme for multi-area power system under cyber-attacks and time-varying delays," *IEEE Trans. Power Syst.*, vol. 38, no. 2, pp. 1336–1349, Mar. 2023.

[32] G. Liu, E. Tian, and X. Xie, "Critical-metrics-based attack strategy and resilient H_∞ state estimator design for multi-area power systems," *IEEE Trans. Smart Grid*, early access, Sep. 5, 2024, doi: 10.1109/TSG.2024.3454637.

[33] Z. Zhang, J. Hu, J. Lu, J. Cao, and F. E. Alsaadi, "Preventing false data injection attacks in LFC system via the attack-detection evolutionary game model and KF algorithm," *IEEE Trans. Netw. Sci. Eng.*, vol. 9, no. 6, pp. 4349–4362, Nov./Dec. 2022.

[34] S. Shi, Z. Fei, H. R. Karimi, and H.-K. Lam, "Event-triggered control for switched T–S fuzzy systems with general asynchronism," *IEEE Trans. Fuzzy Syst.*, vol. 30, no. 1, pp. 27–38, Jan. 2022.

[35] X. Wang, J. Liu, H.-K. Lam, and J. Yu, "Fuzzy-model-based dynamic event-triggered control in sensor-to-controller channel for nonlinear strict-feedback system via command filter," *IEEE Trans. Fuzzy Syst.*, vol. 31, no. 8, pp. 2761–2772, Aug. 2023.

[36] H. Li, X. Jing, H.-K. Lam, and P. Shi, "Fuzzy sampled-data control for uncertain vehicle suspension systems," *IEEE Trans. Cybern.*, vol. 44, no. 7, pp. 1111–1126, Jul. 2014.

[37] X. Sun, Z. Gu, F. Yang, and S. Yan, "Memory-event-trigger-based secure control of cloud-aided active suspension systems against deception attacks," *Inf. Sci.*, vol. 543, pp. 1–17, Jan. 2021.